Chemical Engineering Journal 229 (2013) 540–546

Contents lists available at SciVerse ScienceDirect

Chemical Engineering Journal

journal homepage: www.elsevier.com/locate/cej

Continuous gas-phase synthesis of graphene nanoflakes hybridized by gold nanocrystals for efficient water purification and gene transfection

Jeong Hoon Byeon [a], Young-Woo Kim [b,*]

[a] Department of Chemistry, Purdue University, IN 47907, United States
[b] Department of Automotive Engineering, Hoseo University, Asan 336-795, Republic of Korea

HIGHLIGHTS

- A continuous gas-phase synthesis of gold-reduced graphene oxide (rGO) hybrid nanoflakes was employed.
- Spark discharge produced gold nanocrystals were deposited on rGO nanoflakes during atomization process.
- The ability to achieve dye degradation and gene transfection was greater than that of commercial materials.

GRAPHICAL ABSTRACT

Continuous gas-phase hybridization was employed to prepare gold-reduced graphene oxide hybrid nanoflakes as potential materials for efficient water purification and gene transfection.

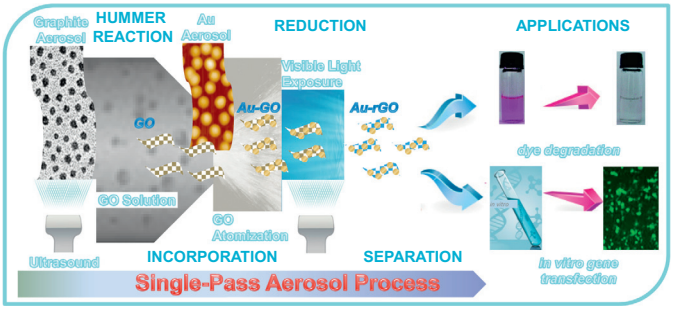

ARTICLE INFO

Article history:
Received 26 April 2013
Received in revised form 10 June 2013
Accepted 15 June 2013
Available online 26 June 2013

Keywords:
Reduced graphene oxide
Gold nanocrystals
Gas-phase process
Hybrid nanoflakes
Dye degradation
Gene transfection

ABSTRACT

The present work reports for the first time a preparation of reduced graphene oxide (rGO) *via* a gas-phase process where a visible light photocatalytic reduction of GO with the use of gold (Au) nanocrystals was performed in a single-pass configuration. Primary Au crystals (~4 nm in diameter) were quantitatively incorporated with GO (~36 nm in lateral dimension) in the form of Au–GO hybrid nanoflakes (~37 nm in lateral dimension). The hybrid flakes were then photocatalytically reduced into a form of Au–rGO, and thus the size and structure of the hybrid flakes were reduced (~32 nm in lateral dimension) and changed (the ratio between the *D* and *G* bands increased from 0.82–1.10). The Au–rGO hybrid flakes were finally employed to degrade dye and transfect into cells *in vitro*, and the ability to achieve dye degradation and gene transfection was greater than that of commercial materials.

1. Introduction

Graphene has attracted much interest for its unique physical and chemical properties and wide-ranging technological applications [1–3]. In the preparation of graphene, the method of utilizing graphene oxide (GO) as a precursor has been widely used [2]. GO is an oxidized form of graphene with phenol hydroxyl and epoxide groups on the basal plane and carboxylic groups at the edges, and normally produced through processing graphite under oxidative conditions. Meanwhile, the reduction of GO has been widely used to prepare graphene [more accurately called reduced GO (rGO)], by methods such as chemical, thermal, flash, laser, or electrochemical reduction [1]. Among these methods, chemical reduction is considered to be the most effective and economical way to prepare rGO from GO. However, chemical reduction usually

* Corresponding author. Tel.: +82 41 540 5819; fax: +82 41 540 5818.
E-mail address: ywkim@hoseo.edu (Y.-W. Kim).

1385-8947/$ - see front matter © 2013 Elsevier B.V. All rights reserved.
http://dx.doi.org/10.1016/j.cej.2013.06.034

requires toxic chemicals, several tedious batch steps, high temperatures and energies, and special instruments and controls for the preparation of rGO, which limits its practical applications [1,4].

Photocatalytic reduction of GO has recently been proven to be an effective method to produce rGO [1]. Compared with conventional chemical reduction, the photoreduction of GO is green and easy to control *via* UV irradiation [5,6], and it often requires semiconductor nanoparticles with large band gaps such as TiO_2 and ZnO, used as photocatalysts, to accelerate the reduction. More recently, the surface plasmon resonance effect of noble metal nanoparticles on photocatalysis has attracted renewed interest, and it has been well established that GO with noble metal nanoparticles can be used as highly active photocatalysts in the presence of an electron donor [1,7,8].

Interest in nanocomposites or hybrid nanomaterials has been ever-growing, ascribed to their peculiarities in combining the desirable properties of building blocks for a given application [9]. Besides the applications of GO and rGO, it is a great desire to fabricate composites or hybrid materials which integrate GO or rGO with nanoparticles, polymers, or even nanotubes and fullerenes [10]. It is of great importance to bind metal nanoparticles onto GO or rGO because the combination and interaction between nanoparticles and GO or rGO will lead to multifunctional or even completely new properties in such a nanocomposite [11]. Metal nanoparticles incorporating GO were recently introduced as materials for antimicrobial [12], biosensor [13], and energy applications [14]. However, the metal hybridization of GO or rGO also requires additional chemical steps and controls for the preparation of metal nanoparticles [9,15], and thus it is still a challenge to prepare metal–(r)GO hybrid particles from raw graphite under continuous conditions.

The present work introduces continuous gas-phase approach for synthesizing gold (Au) decorated rGO hybrid nanoflakes and their applications for dye degradation and gene transfection *in vitro*. Freshly spark produced graphite nanoparticles were first immersed in an ultrasound-impinging device containing a simplified Hummer solution to form GO [4]. The reacted solution containing GO was injected into the reservoir of a collison atomizer. Another spark discharge generated Au nanocrystals, and the particle-laden flow passed over the collison atomizer orifice where they mixed with the atomized GO solution to form hybrid droplets. The droplets then passed through a denuder to drive solvent from the droplets, resulting in AuGO hybrid nanoflakes. The hybrid flakes were then immersed in another ultrasound-impinging device filled with ethanol to photocatalytically form Au–rGO hybrid nanoflakes under visible light. The hybrid nanoflakes were separated using a microfiltration kit, and finally they were applied to dye photodegradation and *in vitro* gene transfection measurements in mammalian cells. An electrical discharge as a graphite supplier was recently employed to prepare graphene nanoflakes [16], while a gas-phase process was also introduced to fabricate graphene with a unique structure [17]. These studies were the motivation to prepare Au–rGO by continuous gas-phase approach, and in addition there was no study to fabricate metal–rGO hybrid nanoflakes in a green and sustainable manner, although it has potential for a broad range of practical applications.

2. Experimental

Graphite nanoparticles were produced *via* spark discharge [18], and carried by nitrogen gas (99.9999% purity, 3 L min^{-1}) to an impinging device, as shown in Fig. 1. The specifications of the discharge configuration were as follows: electrode diameter (C-072561, Nilaco, Japan) and length, 3 mm and 100 mm, respectively; resistance, 0.5 MΩ; capacitance, 1.0 nF; loading current, 2.0 mA; applied voltage, 3.0 kV; and frequency, 667 Hz. The impinging device, which contained a simplified Hummer's solution [4] and an ultrasound probe, was used to collect the graphite particles into the solution and react subsequently with the solution to form GO. The graphite particles experienced ultrasound (250 W cm^{-2} in intensity) when they reached the gas (the graphite particle laden flow)–liquid (the simplified Hummer's solution in the impinging device) interface. GO was obtained by oxidation of the graphite particles (which acted as precursors) with 40 mL of H_2SO_4 and 1.8 g of $KMnO_4$. The residence time of the graphite particles in the impinging device was 3.8 min to form GO. The solution containing GO was injected into the reservoir of a collison atomizer using a peristaltic pump (323Du/MC4, Watson-Marlow Bredel Pump, US).

Another spark discharge between gold rods (AU-172561, Nilaco, Japan) was used to produce Au nanocrystals, and the particle laden flow was employed as the operating gas for atomizing the GO solution supplied by the pump. The Au crystals passed over the atomizer orifice, where they mixed with atomized GO droplets to form hybrid droplets. The droplets then passed through a denuder containing activated carbon pellets and silica gels to drive solvent from the droplets. The resulting aerosol Au–GO hybrid flakes were then injected into another impinging device containing ethanol with an ultrasound probe under visible light to photocatalytically form Au–rGO.

When Au nanocrystals are attached onto GO, a quasi-fermi level forms in the Au–GO flakes. The Au nanocrystals absorb visible light intensely because of the surface plasmon resonance effect, leading to an enhancement of the local electromagnetic fields near the rough Au surface by photoexcited metallic electrons and holes [1]. In the presence of ethanol the holes are scavenged to produce ethoxy radicals, thus leaving the electrons to accumulate within the Au crystals. The accumulated electrons serve to interact with the GO in order to reduce certain functional groups (Eq. (1)).

$$\mathrm{Au} + h\nu \rightarrow \mathrm{Au}(h + e) \xrightarrow{C_2H_5OH} \mathrm{Au}(e) + {}^{\cdot}C_2H_4OH + H^+$$

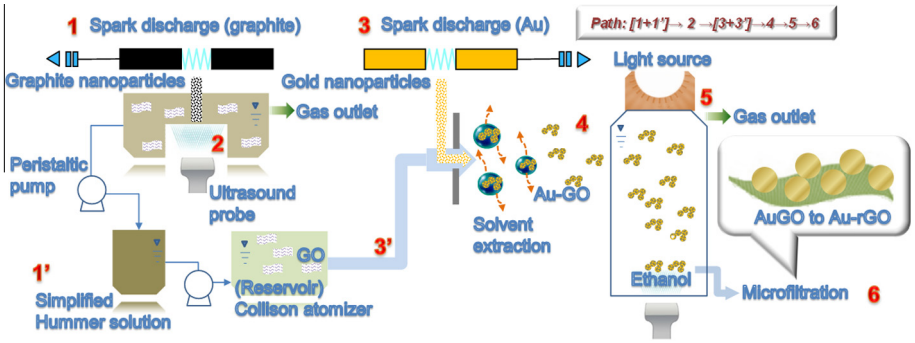

Fig. 1. Continuous gas-phase synthesis of Au–rGO using a serial reactor consisting of spark discharges, ultrasound probe inserted impingers, and a collison atomizer.

$$Au(e) + GO \rightarrow Au + rGO \quad (1)$$

After the photocatalytic reduction procedure, Au–rGO hybrid nanoflakes were separated from the solution using a microfiltration unit (33980, Corning, US) with a polytetrafluoroethylene (PTFE) membrane substrate (11807-47-N, Sartorius, Germany). The hybrid flakes were rinsed with deionized water after they were separated from the solution to remove the residual, then were set aside to dry in a clean booth to keep them in a powder form. The nanoflakes were detached from the PTFE substrate by immersing the sample in solvent and subjecting them to ultrasound treatment for 10 s right before being applied for the purposes of photocatalytic dye degradation and *in vitro* gene transfection.

Photocatalytic degradation of rhodamine B (RhB) in the presence of Au–rGO was investigated by irradiating aqueous solutions of the dye molecule (10 mL, 10^{-4} M) containing suspended Au–rGO nanoflakes (0.4 mg mL^{-1}) with visible light (*via* a Xenon lamp equipped with a 420 nm cut-off filter) while stirring with a magnetic bar. For comparison purposes, photocatalytic reduction of RhB was also carried out in the presence of titania (P-25, Degussa, Germany) as a reference photocatalyst. The concentration was monitored by UV–vis absorption spectroscopy (330, Perkin–Elmer, US) through changes in the absorption peak at 554 nm.

Human embryonic kidney (HEK) 293 cells were incubated with Au–rGO for 24 h, and cell viability was determined through a standard MTT [3-(4,5-dimethylthiazol-2-yl)-diphenyltetrazolium bromide] assay. Absorbances were measured at 570 nm by an ELISA plate reader (Thermo Multiskan Spectrum, US). The percentage cell viability was related to the untreated control cells. The ability of the Au–rGO to transfect HEK 293 cells was next examined using plasmid DNA that contain the luciferase and enhanced green fluorescent protein (EGFP) gene. Luciferase activity was measured with a luminometer (TD-20/20, Promega, US). The final luciferase activity was expressed in RLU mg^{-1} of protein. An inverted fluorescent microscope (DMI 4000 B, Leica, Germany) was used to observe the EGFP expression of the polyplexes in the 293 cells.

3. Results and discussion

To prepare GO, first graphite nanoparticles were produced by spark discharge. The gas temperature inside the spark channel was increased beyond a critical value, which was sufficient to sublimate parts of the graphite electrodes [19]. The duration of each spark was very short (~1 ms) and the vapors cooled rapidly downstream of the spark. This formed a supersaturation resulting particle formation through nucleation–condensation. The total number

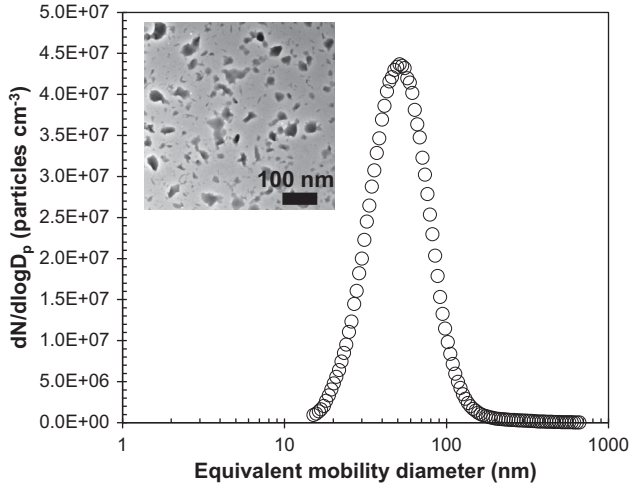

Fig. 2. A size distribution of aerosol graphite particles with a TEM image.

Table 1
A summary of the gas-phase size distributions of graphite particles, Au nanocrystals, and GO and Au–GO nanoflakes.

Case	GMD (nm)	GSD (–)	TNC ($\times 10^6$ particles cm^{-3})
Graphite	50.7	1.54	20.0
Au	24.0	1.50	8.32
GO	36.2	1.57	2.74
Au–GO	37.0	1.61	3.90

concentration (TNC), geometric mean diameter (GMD), and geometric standard deviation (GSD) of the graphite particles, which were measured using a scanning mobility particle sizer (3936, TSI, US), were 2.00×10^7 particles cm^{-3}, 50.7 nm, 1.54, respectively, as shown in Fig. 2. Fig. 2 also shows a transmission electron microscope (TEM, JEM-3010, JEOL, Japan) image of the graphite particles. The mean mode diameter of the graphite particles was 56 ± 5.5 nm, and this is consistent with the size distribution in gas-phase described in Table 1. The produced graphite particles were carried using a flow of nitrogen gas and then collected in the simplified Hummer's solution by means of ultrasound.

Au–GO hybrid flakes were formed by incorporating Au with GO during the atomization of the GO solution. We verified a mergence between the Au and GO by measuring the size distributions of the Au, GO, and Au–GO in gas-phase. Fig. 3a summarizes the size distribution measurements of the Au–GO flakes. The GMD, GSD, and TNC of the Au–GO flakes were 37.0 nm, 1.61, and 3.90×10^6 particles cm^{-3}, respectively. The analogous data for Au were 24.0 nm, 1.50, 8.32×10^6 cm^{-3}, respectively, and for GO were 36.2 nm, 1.57, 2.74×10^6 particles cm^{-3}, respectively. The size distribution of the Au–GO was rather similar to the GO flakes compared to that of the Au crystals, and there was no bimodal distribution character, implying that the Au crystals were nearly quantitatively incorporated with the GO, to form Au–GO hybrid flakes. Fig. 3b shows the collection efficiency of the Au–GO flakes to be photocatalytically reduced in the impinging device at 250 W cm^{-2} of ultrasound intensity under visible light. The Au–GO flakes experienced ultrasound streaming at the gas–liquid interface and about 96% of the particles were collected in the ethanol solution, because the force on the interface could give rise to a particle velocity (U_{as}) in accordance with the following equation [20]:

$$U_{as} = \left(\frac{2P\beta}{\rho_g c_s \pi \alpha^2 X}\right)^{1/2} \quad (2)$$

where P is the acoustic power of the ultrasound, β is the acoustic energy attenuation coefficient, ρ_g is the gas density, c_s is the sonic velocity in gas, α is the semi-angle of the spread of the streaming, and X is the distance from the source. Collection efficiencies increased linearly when the Stokes parameter (Eq. (3)) increased,

$$Stk^{1/2} = \left(\frac{C_c \rho_p U_{as} D_p}{9\mu\xi}\right)^{1/2} \quad (3)$$

where Stk is the Stokes number, C_c is the slip correction factor, ρ_p is the particle density, D_p is the particle diameter, μ is the gas viscosity, and ξ is the oscillation amplitude. The collection of <30 nm particles was not significantly decreased although the particles of <30 nm may be governed by a diffusional motion for the conventional impactors. This may have originated from different mechanisms of the particle attachment on their counter media between the present [the particles in a bubble attached on the liquid surface by bubble collapsing (refer inset of Fig. 3b) due to ultrasound streaming] and conventional (the particles in gas attached on a solid plate by inertial impaction) methods [21]. The plots were generated by dividing the output and input aerosol size distribution. The plots show that a decrease in collection efficiency by decreasing size was probably due to a decrease of the attachment frequency between

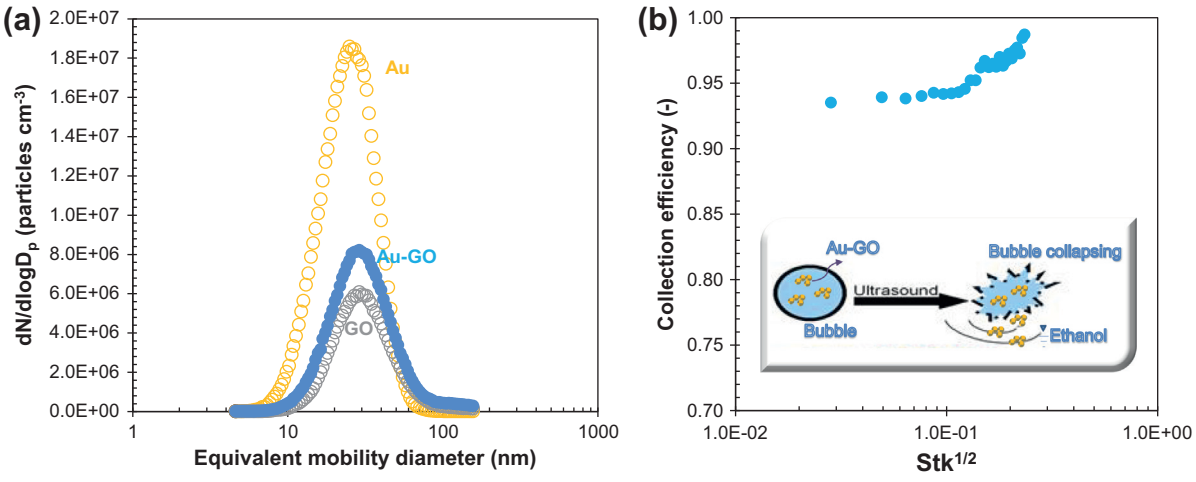

Fig. 3. (a) Gas-phase size distributions of Au nanocrystals and GO and Au–GO nanoflakes. (b) The collection efficiency of the Au–GO nanoflakes by an ultrasound impinging device. This figure also shows a schematic (inset) of Au–GO collection by bubble collapsing in the presence of ultrasound.

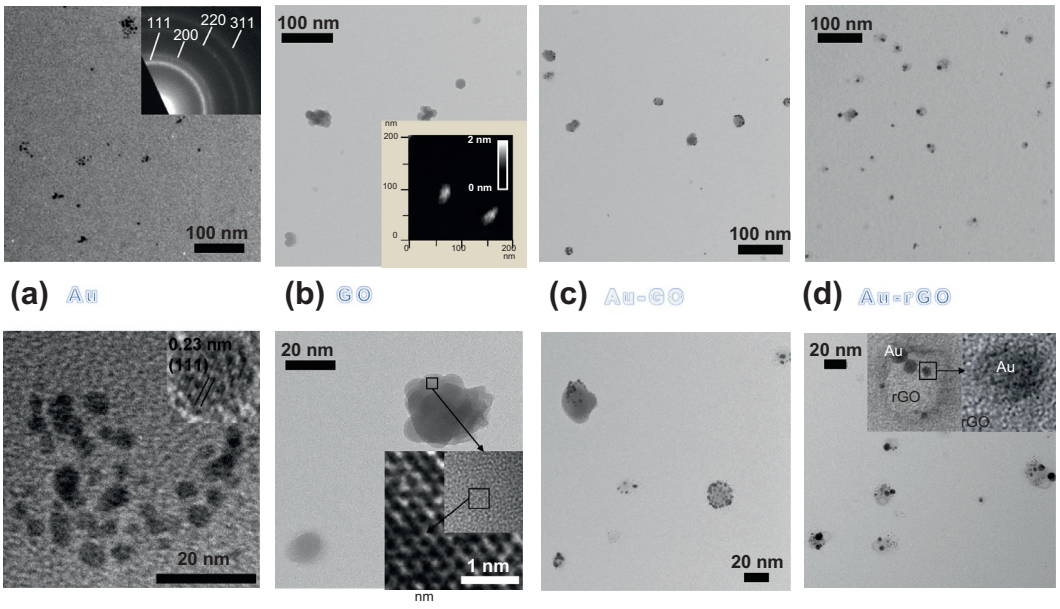

Fig. 4. TEM images of samples of (a) Au nanocrystals and (b) GO, (c) Au–GO and (d) Au–GO nanoflakes after a photocatalytic reduction (i.e. Au–rGO). The AFM image of GO is also displayed in (b).

the particle and the liquid surface (i.e. increasing distances between the particle and the surface).

Low and high magnification TEM images show the morphology of Au, GO, and Au–GO samples. The TEM images (Fig. 4a) reveal that the Au crystals were agglomerates of several primary particles (each ~4 nm in diameter). Fig. 4a also shows the electron diffraction pattern corresponding to the TEM micrograph. The pattern has a sharp diffraction line showing the (111) reflection, and also weak diffraction lines showing the (200) and (220) reflections of the face-centered cubic lattice for metallic Au, which indicates that the crystals grew predominantly along the (111) lattice and mostly consisted of several nanometer sized crystallites. The morphology of the GO flakes was as flakes, and a high resolution TEM image (inset of Fig. 4b) of the GO shows a regular hexagonal structure as expected for graphene, while several internal defects could also be found within the structure. Fig. 4b also shows a representative atomic force microscope (IIIa, NanoScope, US) image of the GO particles on a silicon substrate. The particle size was about 35 nm, with an apparent thickness of about 1 nm, which indicates that they consist of single graphene layers. When the Au crystals passed over the orifice of the collison atomizer, most Au crystals were attached to the GO flakes, resulting in Au–GO flakes (Fig. 4c). Moreover, the Au crystals were redistributed on the GO flakes due to deagglomeration (by setting the force acting on an agglomerate of size D_{pa} due to the sudden pressure change across an orifice in the collison atomizer) [22–26], and the size is given by:

$$D_{pr} = \alpha\sqrt{\frac{D_{pa}H}{6\pi\Delta P\Theta^2}} \quad (4)$$

where D_{pr} is the size of a restructured agglomerate, α is the proportionality constant, H is the Hamaker constant, ΔP is the pressure difference between the front and the rear of the orifice, and Θ is the parameter controlling the maximum cohesive strength between the constituting particles in an agglomerate. Au agglomerates pass through the orifice, and the rapid changes in pressure, density, and velocity across the orifice produce an impulse capable of shattering the agglomerates. Fig. 4d shows the Au–GO hybrid

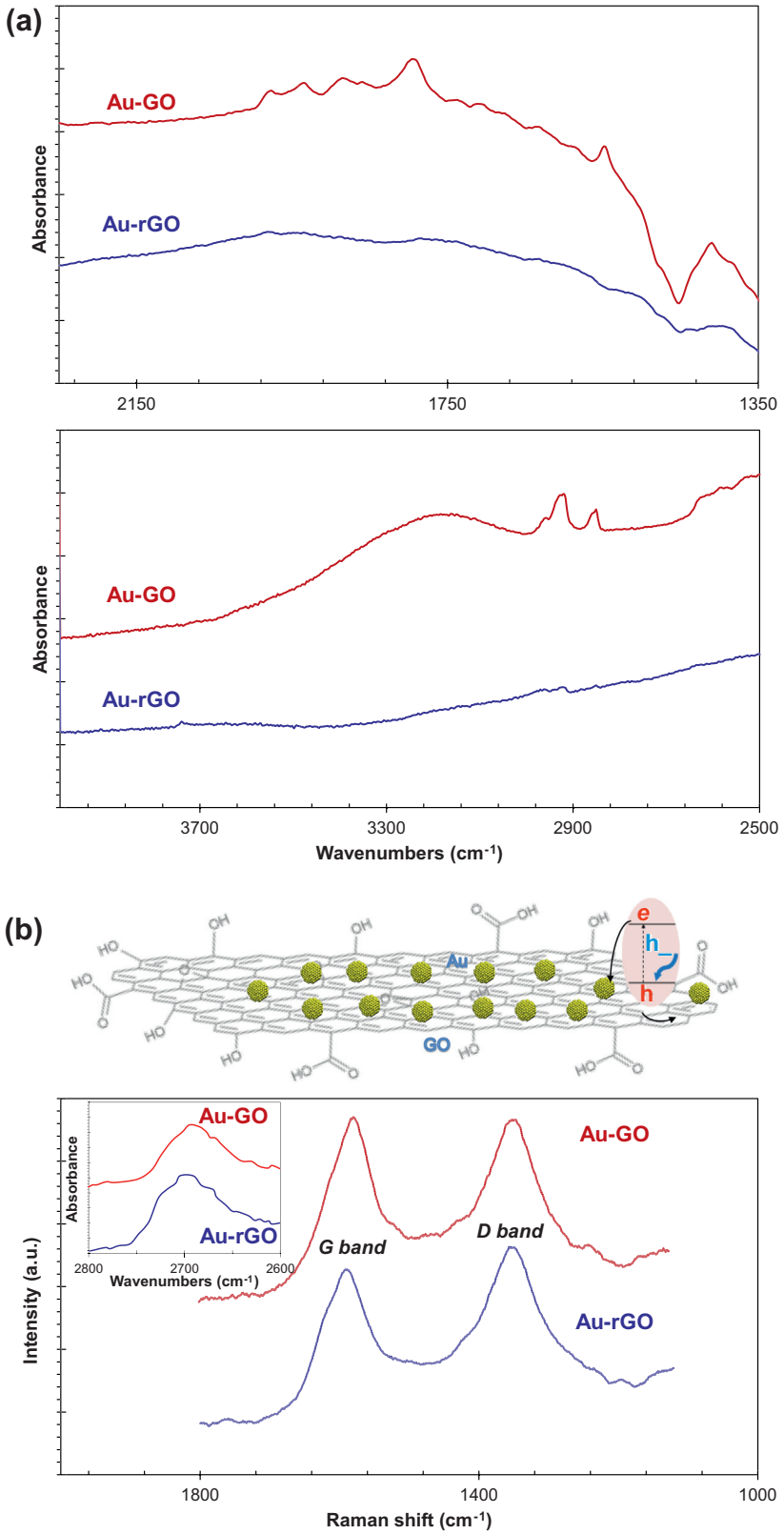

Fig. 5. (a) FTIR and (b) Raman spectra of the Au–GO and Au–rGO nanoflakes.

flakes after photocatalytic reduction in the presence of ethanol under visible light. There were no significant differences in the morphology before and after the reduction, but the mean mode diameter of the Au–GO decreased from ~37 nm to ~33 nm, and they became brighter after the reduction. Interestingly, even after a photocatalytic reduction in the presence of ultrasound, the Au crystals were still anchored on the surface of the rGO, implying a strong interaction between the Au and the rGO.

Fourier transform infrared (FTIR) spectroscopy (Nicolet 6700, Thermo Electron, US) was used to verify the reduction of GO. In

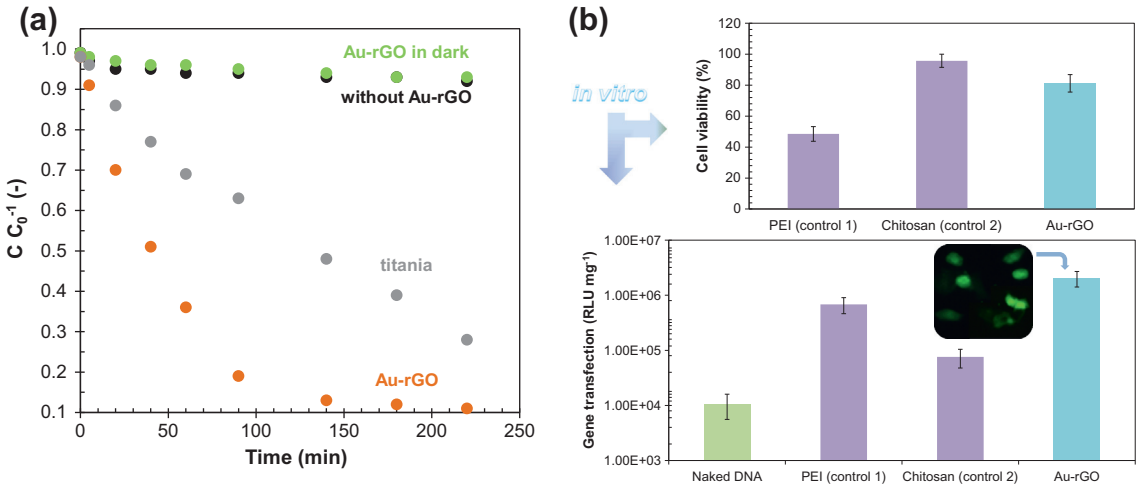

Fig. 6. (a) Photocatalytic degradation of RhB with Au–rGO hybrid nanoflakes. (b) *In vitro* measurements of cell viability and gene transfection efficiency for Au–rGO hybrid nanoflakes.

Fig. 5a, the peak around at 1730 cm^{-1} was characteristic of C═O in carboxylic acid and carbonyl moieties on the surface of the GO, and the peaks at 1620, 1,410, and 1,380 cm^{-1} were due to aromatic C═C, carboxy C—O, and O—H groups, respectively. Other features include characteristic absorption peaks at around 3300 cm^{-1} (related to O—H groups), 2940 cm^{-1} (CH_2 bend), and 2960 cm^{-1} (CH_3 bend). Comparing it with GO, rGO shows a featureless spectrum at the given absorbance scales, implying a reduction in the amount of oxygen functionalities. The structural changes occurring during the reduction are also reflected in the Raman spectra (T64000, HORIBA Jobin Yvon, Japan) (Fig. 5b). The spectra showed an increase in the ratio between the *D* and *G* bands (I_D/I_G), indicating an increased number of defects or edge areas from GO to rGO. The intensity of the overtone 2*D* band (inset) with respect to the *D* and *G* peaks is small. After the phototreatment, there is a small peak shift for the 2*D* band and no obvious shift for the *D* band and *G* band. The 2*D* band peak of GO shifted from at 2686 cm^{-1} to at 2692 cm^{-1} after the phototreatment. The shift of the peak position of the 2*D* band is indicative of reduction of GO (refer the upper image of Fig. 5b). According to a report by Stankovich et al. [27], moreover, the increase in the I_D/I_G ratio from 0.82 to 1.10 is because the new graphitic domains created during the reduction of GO to rGO are smaller in size (i.e. smaller in-plane sp^2 domains are formed) than the size of the GO before reduction. Therefore, the decreased average size of the rGO makes the I_D/I_G ratio increase, and this is consistent with the TEM measurements (Fig. 4c and d). In addition, the smaller size of the rGO will result in a large quantity of edges. The edges will act as defects, resulting in an increase in the *D* band.

Fig. 6a plots the relative changes in the concentration of aqueous RhB solution as a function of the reaction time. It can be seen that RhB was very stable under visible light irradiation without a catalyst, or in the presence of Au–rGO in the dark. Photodegradation of the dye was prompted by the Au–rGO, and it could also be achieved in the presence of titania. The rate constant was calculated to be about 9.1×10^{-3} min^{-1}, greater than that of titania (2.6×10^{-3} min^{-1}) and even larger than that mentioned in a previous report [7]. The enhancement was probably due to the smaller sizes of both Au (~4 nm) and rGO (~33 nm) [28] than the sizes (>5 nm for Au, several microns for rGO) in the previous report. The dye was first excited to ·dye followed by an electron transfer from the ·dye to the rGO. Owing to the interaction (electrostatic attraction and π–π interaction) between the dye molecules and the rGO, the dye molecules are expected to readily adsorb onto the rGO [8]. The electron then moved to a Au crystal and was trapped by oxygen to produce various reactive oxygen species (ROS), and the ROS finally degraded the dye.

We tested the cytotoxicity and gene transfection properties of the Au–rGO flakes as a potential material for biomedical applications. The results (Fig. 6b) show that the cell viability was ~82% for the Au–rGO, while the measured viabilities of the PEI and chitosan control systems were ~49% and ~96%, respectively. This implies that the Au–rGO has a biocompatibility that may be suitable in a clinical context. The transfection efficiencies of Au–rGO/pDNA (2.1×10^6 RLU mg^{-1} protein) complexes in the HEK 293 cell line were higher than that of naked DNA (1.1×10^4) (Fig. 6b). Out of these, the efficiency for the Au–rGO was the highest, even higher than those of chitosan (7.6×10^4) and PEI (6.8×10^5). The inset of Fig. 6b shows the fluorescence of HEK 293 cells for the Au–rGO derived from the EGFP expression, which further confirmed the transfection. The higher efficiency of the Au–rGO could be related to the particle size (35 nm: Au–rGO < 120 nm: PEI < 165 nm: chitosan) of the sample/pDNA complexes [29]. This implies that the transfection efficiency may be controlled by differentiating the material structures. In a previous report, gene carriers with smaller sizes below 100 nm have been shown to have significantly higher transfection efficiencies than those of larger sizes [30].

4. Conclusions

Continuous gas-phase process was developed to fabricate Au–rGO hybrid nanoflakes in a continuous, green, and generalizable configuration. The prepared hybrid nanoflakes were briefly applied to the photodegradation of dye and gene transfection *in vitro* to verify their potentials in the environmental and biomedical fields. The proposed method not only provides an on-demand photoreduction technique but also opens up a new way to obtain photoactive metal–rGO hybrid nanoflakes for a broad range of practical applications.

References

[1] T. Wu, S. Liu, Y. Luo, W. Lu, L. Wang, X. Sun, Surface plasmon resonance-induced visible light photocatalytic reduction of graphene oxide: using Ag nanoparticles as a plasmonic photocatalyst, Nanoscale 3 (2011) 2142–2144.

[2] Y. Pan, H. Bao, L. Li, Noncovalently functionalized multiwalled carbon nanotubes by chitosan-grafted reduced graphene oxide and their synergistic reinforcing effects in chitosan films, ACS Appl. Mater. Interfaces 3 (2011) 4819–4830.
[3] Y.H. Ding, P. Zhang, Q. Zhuo, H.M. Ren, Z.M. Yang, Y. Jiang, A green approach to the synthesis of reduced graphene oxide nanosheets under UV irradiation, Nanotechnology 22 (2011) 215601.
[4] H.N. Lim, N.M. Huang, C.H. Loo, Facile preparation of graphene-based chitosan films: enhanced thermal, mechanical and antibacterial properties, J. Non-Cryst. Solids 358 (2012) 525–530.
[5] G. Štengl, D. Popelková, P. Vláčil, TiO_2-graphene nanocomposite as high performace photocatalysts, J. Phys. Chem. C 115 (2011) 25209–25218.
[6] O. Akhavan, Photocatalytic reduction of graphene oxides hybridized by ZnO nanoparticles in ethanol, Carbon 49 (2011) 11–18.
[7] Z. Xiong, L.L. Zhang, J. Ma, X.S. Zhao, Photocatalytic degradation of dyes over graphene–gold nanocomposites under visible light irradiation, Chem. Commun. 46 (2010) 6099–6101.
[8] L. Guardia, S. Villar-Rodil, J.I. Paredes, R. Rozada, A. Martínez-Alonso, J.M.D. Tascón, UV light exposure of aqueous graphene oxide suspensions to promote their direct reduction, formation of graphene–metal nanoparticle hybrids and dye degradation, Carbon 50 (2012) 1014–1024.
[9] J. Shen, M. Shi, B. Yang, H. Ma, N. Li, M. Ye, One-pot hydrothermal synthesis of Ag-reduced graphene oxide composite with ionic liquid, J. Mater. Chem. 21 (2011) 7795–7801.
[10] X. Zhou, X. Huang, X. Qi, S. Wu, C. Xue, F.Y.C. Boey, Q. Yan, P. Chen, H. Zhang, In situ synthesis of metal nanoparticles on single-layer graphene oxide and reduced graphene oxide surfaces, J. Phys. Chem. C 113 (2009) 10842–10846.
[11] Z. Jin, D. Nackashi, W. Lu, C. Kittrell, J.M. Tour, Decoration, migration, and aggregation of palladium nanoparticles on graphene sheets, Chem. Mater. 22 (2010) 5695–5699.
[12] J. Ma, Z. Zhang, Z. Xiong, Y. Yong, X.S. Zhao, Preparation, characterization and antibacterial properties of silver-modified graphene oxide, J. Mater. Chem. 21 (2011) 3350–3352.
[13] Y. Wan, Y. Wang, J. Wu, D. Zhang, Graphene oxide sheet-mediated silver enhancement for application to electrochemical biosensors, Anal. Chem. 83 (2011) 648–653.
[14] X.-J. Lv, W.-F. Fu, H.-X. Chang, H. Zhang, J.-S. Cheng, G.-J. Zhang, Y. Song, C.-Y. Hu, J.-H. Li, Hydrogen evolution from water using semiconductor nanoparticle/graphene composite photocatalysts without noble metals, J. Mater. Chem. 22 (2012) 1539–1546.
[15] Y. Guo, X. Sun, Y. Liu, W. Wang, H. Qiu, J. Gao, One pot preparation of reduced graphene oxide (RGO) or Au (Ag) nanoparticle-RGO hybrids using chitosan as a reducing and stabilizing agent and their use in methanol electrooxidation, Carbon 50 (2012) 2513–2523.
[16] Z.-S. Wu, W. Ren, L. Gao, J. Zhao, Z. Chen, B. Liu, D. Tang, B. Yu, C. Jiang, H.-M. Cheng, Synthesis of graphene sheets with high electrical conductivity and good thermal stability by hydrogen arc discharge exfoliation, ACS Nano 3 (2009) 411–417.
[17] J. Luo, H.D. Jang, T. Sun, L. Xiao, Z. He, A.P. Katsoulidis, M.G. Kanatzidis, J.M. Gibson, J. Huang, Compression and aggregation-resistant particles of crumpled soft sheets, ACS Nano 5 (2011) 8943–8949.
[18] J.H. Byeon, J.H. Park, K.Y. Yoon, B.J. Ko, J.H. Ji, J. Hwang, Removal of volatile organic compounds by spark generated carbon aerosol particles, Carbon 44 (2006) 2106–2109.
[19] J.H. Byeon, J.-W. Kim, Production of carbonaceous nanostructures from a silver–carbon ambient spark, Appl. Phys. Lett. 96 (2010) 153102.
[20] J.H. Byeon, Y.-W. Kim, An aerosol-seed-assisted hybrid chemical route to synthesize anisotropic bimetallic nanoparticles, Nanoscale 4 (2012) 6726–6729.
[21] D. Park, N.-K. Choi, S.-G. Lee, J. Hwang, Real-time measurement of the size distribution of diesel exhaust particles using a portable 4-stage electrical low pressure impactor, Part. Part. Syst. Charact. 26 (2009) 179–186.
[22] J.H. Byeon, J.T. Roberts, Aerosol based fabrication of biocompatible organic–inorganic nanocomposites, ACS Appl. Mater. Interfaces 4 (2012) 2693–2698.
[23] J.H. Byeon, J.-W. Kim, Aerosol fabrication of thermosensitive nanogels and in situ hybridization with iron nanoparticles, Appl. Phys. Lett. 101 (2012) 023117.
[24] J.H. Byeon, Y.-W. Kim, Gas-phase self-assembly of highly ordered titania@graphene nanoflakes for enhancement in photocatalytic activity, ACS Appl. Mater. Interfaces 5 (2013) 3959–3966.
[25] J.H. Byeon, Y.-W. Kim, Continuous gas-phase synthesis of metal oxide–graphene hybrid nanoflakes for the enhancement of lithium storage, RSC Adv. 3 (2013) 7259–7264.
[26] J.H. Byeon, Y.-W. Kim, Hybrid gas-phase synthesis of nanoscale Fe-SiO_2 core-shell agglomerates for efficient transfection into cell and use in magnetic cell patterning, RSC Adv. 3 (2013) 3, http://dx.doi.org/10.1039/c3ra42151a.
[27] S. Stankovich, D.A. Kikin, R.D. Piner, K.A. Kohlhaas, A. Kleinhammes, Y. Jia, Y. Wu, S.T. Nguyen, R.S. Ruoff, Synthesis of graphene-based nanosheets via chemical reduction of exfoliated graphite oxide, Carbon 45 (2007) 1558–1565.
[28] H.-I. Kim, G.-H. Moon, D. Monllor-Satoca, Y. Park, W. Choi, Solar photoconversion using graphene/TiO_2 composites: nanographene shell on TiO_2 core versus TiO_2 nanoparticles on graphene sheet, J. Phys. Chem. C 116 (2012) 1535–1543.
[29] J.H. Byeon, J.T. Roberts, Aerosol based fabrication of thiol-capped gold nanoparticles and their application for gene transfection, Chem. Mater. 24 (2012) 3544–3549.
[30] J.H. Byeon, H.-K. Kim, J.T. Roberts, Monodisperse poly(lactide-co-glycolic acid)-based nanocarriers for gene transfection, Macromol. Rapid Commun. 33 (2012) 1840–1844.